Solar Energy Materials & Solar Cells 133 (2015) 105–112

Contents lists available at ScienceDirect

Solar Energy Materials & Solar Cells

journal homepage: www.elsevier.com/locate/solmat

Investigating the charge transport kinetics in poly-crystalline silicon solar cells for low-concentration illumination by impedance spectroscopy

Pankaj Yadav [a], Brijesh Tripathi [a,b], Kavita Pandey [a], Manoj Kumar [b,*]

[a] School of Solar Energy, Pandit Deendayal Petroleum University, Gandhinagar 382007, India
[b] School of Technology, Pandit Deendayal Petroleum University, Gandhinagar 382007, India

ARTICLE INFO

Article history:
Received 12 November 2013
Received in revised form
14 October 2014
Accepted 21 October 2014
Available online 21 November 2014

Keywords:
Low-concentration photovoltaic (LCPV)
Poly-crystalline silicon solar cell
Carrier density
Recombination kinetics
Diffusion resistance

ABSTRACT

Commercially available polycrystalline silicon solar cells have been studied under varying illumination conditions to evaluate their application in low-concentration photovoltaic systems. The present work explores a detailed analytical framework for determining a broad range of performance indicating parameters for polycrystalline silicon solar cells by using the impedance spectroscopy (IS) technique. The IS measurements show that the diffusion capacitance varies from 1×10^{-7} to 5×10^{-7} F/cm^2 and diffusion resistance from 0.5 to 770 Ω-cm^2 with the applied bias. The IS measurements also indicated that the effective lifetime of charge carriers decreases with increasing illumination. This study confirms that commercially available polycrystalline silicon solar cells can work satisfactorily under low concentration (<3.5 suns).

1. Introduction

Solar energy is emerging as a renewable energy source to meet the energy demand of the next generation. The solar energy can be directly utilized for heating/cooling of fluids (i.e. solar thermal), or it can be converted into electrical energy by using solar photovoltaic (PV) cells. The direct conversion of solar radiation into electrical energy is the most suitable way of utilizing solar energy because of its convenience and diverse applications. Among the various existing semiconductor materials, silicon is the most widely used (80–90%) semiconductor for the fabrication of solar cells. At present, the price of electricity generated from silicon solar cells is somewhat higher than conventional energy sources. Further cost reduction of the solar cell is possible by using thin c-Si wafers [1], c-Si thin film [2], Si in the form of ribbon [3,4] and concentrator Si solar cells [5,6]. In the last decade, the price of silicon based solar modules has been drastically reduced making it more productive to develop low-concentration photovoltaic (LCPV) systems using these cells to achieve grid parity in the near future.

Concentrator photovoltaic (CPV) technologies are usually classified according to their concentration ratio (CR), that is, low, medium and high concentration systems [7,8]. The major challenges at medium and high concentration are: an increase in cell temperature reduces the efficiency and an accurate sun tracking system is required which increases the overall cost of the system [6]. Silicon solar cell based low concentration photovoltaic (LCPV) systems with a CR below 5 suns present two major advantages: first, LCPV systems can use conventional high performance silicon solar cells (made for 1 sun application [9]); and second, LCPV systems are less demanding in terms of tracking accuracy as compared to high concentration systems [10].

Recently, there has been a renewed interest in the low concentration silicon PV systems [11–20]. In this technology, commercial silicon solar cells are used under a concentration of 2 to 10 suns. Improvement in performance is obtained by reducing the series resistance of the solar cells using electro-deposition of high aspect ratio front metal contacts [2]. A detailed review on the modeling of low-concentration solar photovoltaics is presented by Zahedi et al. [12]. Li et al. have studied the performance of solar cell arrays based on a trough concentrating photovoltaic/thermal system [18]. Recently, Schuetz et al. [19] have reported the design and construction of $\sim7\times$ LCPV system based on compound parabolic concentrators.

Most of the studies discussed above have been performed for mono-crystalline silicon based solar cells. There is scarcity of literature on the applicability of polycrystalline silicon solar cells for low-concentration photovoltaic systems. A thorough understanding of electron kinetics is crucial in designing polycrystalline

* Corresponding author. Tel.: +91 79 2327 5428; fax: +91 79 2327 5030.
E-mail address: manoj.kumar@sse.pdpu.ac.in (M. Kumar).

http://dx.doi.org/10.1016/j.solmat.2014.10.031
0927-0248/

solar cells for LCPV applications. Close to zero-bias, the operation of an efficient solar cell is usually determined by charge separation. On the other hand at the maximum power point (close to V_{OC}), recombination kinetics (i.e. the effective recombination lifetime) play a major role [21]. The impedance spectroscopy (IS) technique is used for studying the recombination kinetics through resistance and capacitance measurements. IS is a small perturbation method that resolves the capacitive and resistive elements of electronic devices under test at steady state conditions. In the present article, commercially available polycrystalline silicon solar cells have been studied under varying illumination (i.e. varying concentration ratio, CR < 5 Sun) to find their suitability for low-concentration photovoltaic systems.

2. Theoretical modelling

2.1. Two-diode model of polycrystalline silicon solar cell

The current loss in a solar cell is governed by various recombination mechanisms [22–23] that is, (1) radiative recombination of electron-hole pairs, (2) Shockley-Read-Hall, Auger and surface recombination, (3) series and shunt resistance losses. The two-diode model used here incorporates all the above mentioned loss mechanisms and is shown in Fig. 1. The Diode 1 conducts the current arising due to the diffusion of minority carriers in the quasi neutral region of the solar cell where they recombine. The losses in the depletion region are described by Diode 2, which incorporates defect–induced charge recombination losses in the depletion region. The terminal equation for current-voltage characteristics of the solar cell is given by [24–29]:

$$I = I_{PH} - I_{D1} - I_{D2} - (V + IR_S)/R_{SH} \quad (1)$$

where I_{PH} represents the photocurrent, R_S represents the series resistance and R_{SH} represents the shunt resistance.

The diode current density in the forward bias condition can be expressed in terms of the voltage V as:

$$I_{D1} = I_i\left\{\exp\left(\frac{q(V+IR_S)}{n_1 k_B T}\right) - 1\right\} \quad (2)$$

$$I_{D2} = I_r\left\{\exp\left(\frac{q(V+IR_S)}{n_2 k_B T}\right) - 1\right\} \quad (3)$$

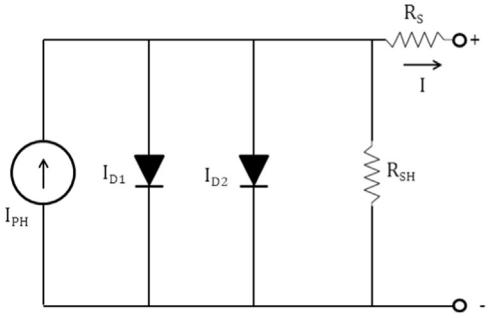

Fig. 1. The standard two diode model of a polycrystalline silicon solar cell.

where I_{D1} and I_{D2} are the current densities of diode 1 and 2 that originate from different carrier recombination mechanisms in the quasi neutral region (QNR) and the space charge region (SCR) respectively, where n_1 and n_2 are the corresponding diode ideality factors.

Generally, for solar cells under zero terminal voltage $I_{PH} \gg I_r$, I_i so in Eq. (1), the small diode currents (I_r and I_i) can be ignored. Therefore the short-circuit current (I_{SC}) is approximately equal to I_{PH}. I_{PH} mainly depends on the solar insolation and cell's working temperature by Eq. (4) [30]:

$$I_{PH} = \left[I_{SC} + K_I(T_C - T_{Ref})\right] \times CR \quad (4)$$

where, CR represents the concentration ratio, K_I is the cell's short-circuit current temperature coefficient, T_{Ref} is the cell's reference temperature and T_C is the cell's working temperature. The maximum power output (P_{MAX}) of the polycrystalline silicon solar cell is related to I_{SC} and open circuit voltage (V_{OC}) through the following equation:

$$P_{MAX} = FF \times V_{OC} \times I_{SC} \quad (5)$$

The values of I_{SC}, V_{OC} and FF can be determined from the I-V characteristics obtained by Eq. (1). The efficiency of the solar cell in relation with P_{MAX} is given by Eq. (6):

$$\eta = \frac{P_{MAX}}{(A \times \lambda)} \quad (6)$$

where, A is the area of solar cell. Based on the model described above, the electrical performance of the polycrystalline silicon solar cell is simulated using MATLAB/Simulink.

2.2. AC equivalent circuit

An AC equivalent circuit is proposed here to understand the recombination kinetics of polycrystalline silicon solar cell under illumination. The distributed elements of the proposed equivalent circuit can provide quantitative information on the diffusion and recombination mechanism associated with polycrystalline silicon solar cell. To derive the complex impedance of transmission line model (Fig. 2), it is assumed that the distributed circuit elements are position independent and charge carriers are homogeneously distributed in the solar cell [31]. The collection of charge carriers across the load terminals is dependent on the active layer thickness (L) of the device and the minority carrier diffusion length (L_n). For efficient charge collection, $L_n \gg L$, whereas the charge collection would be worst if $L_n \ll L$. The elements of the proposed equivalent circuit (Fig. 2) comprises (1) a distributed transfer resistance ($r_{tr} = R_t/L$) responsible for hindrance in the electron transport; (2) a distributed diffusion capacitance ($c_\mu = C_\mu/L$), represents the capacitance per unit area which is associated with the homogeneous accumulation of charge carriers; (3) diffusion resistance ($r_d = R_d/L$), associated with electron-hole recombination in the active layer. The effective net impedance of the above circuit elements is represented by Eq. (7) [21, 31]:

$$Z = \left(\frac{R_t R_d}{1 + i\omega/\omega_{rec}}\right)\coth\left[\left(\frac{\omega_{rec}}{\omega_d}\right)^{1/2}\left(1 + \frac{i\omega}{\omega_{rec}}\right)^{1/2}\right] \quad (7)$$

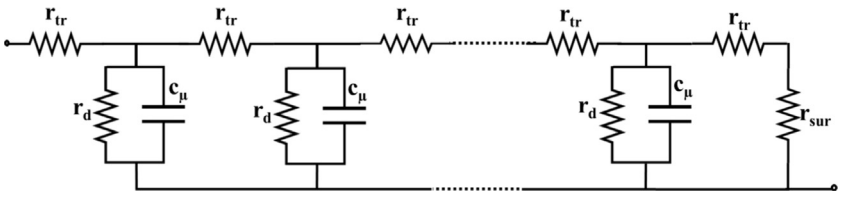

Fig. 2. Equivalent circuit (transmission line model) of polycrystalline silicon solar cell comprising of differential elements related to electron transport resistance (r_{tr}), diffusion resistance (r_d), diffusion capacitance (c_μ) and back-surface recombination resistance ($r_{sur} \to 0$) [21,31].

Here, $\omega_d = D_n/L^2 = 1/R_tC_\mu$ is effective rate constant of diffusion in active layer (D_n being the electron diffusion coefficient), and $\omega_{rec} = 1/R_dC_\mu$ is the effective rate constant of recombination (reciprocal of electron lifetime), ω is the angular frequency and $i = (-1)^{1/2}$. The carrier collection efficiency is governed by L_n, which is related to the recombination characteristic frequency. The high frequency part of the impedance spectra contains information about the transport of charge carriers, series resistance elements and dielectric contributions from the silicon solar cell. The series resistance, R_S is composed of the contributions from front contact grid of silver, back contact of aluminum and carrier transporting interlayer. Interfaces between the active layer and metallic contacts add more resistance in series because of partial energy level alignment, which affects the optimal charge transfer at the interface. The low frequency arc is associated with the diffusion capacitance, diffusion resistance and minority carrier lifetime of the silicon solar cell [21].

The difference between electron and hole Fermi level defines the *upper limit of achievable open-circuit voltage* (V_F) as given by Eq.(8) [21] and shown in Fig. 3:

$$qV_F = E_{Fn} - E_{Fp} \tag{8}$$

At low illumination levels in the case of p-type base material, the hole quasi-Fermi level is almost equal to its equilibrium value $E_{Fp} \approx E_{F0}$ and only a slight occupancy of the conduction band is expected. The occupancy of conduction band electrons, valence band holes and trap states all work in a complex dynamic way during the SRH recombination process. At higher illumination levels (Fig. 4), an increased number of electrons are added to acceptor states and holes are added to donor states, which shifts the electron Fermi level, E_{Fn} toward higher energies, while the hole Fermi level, E_{Fp} undergoes a small downward shift. Due to the change in occupancy of conduction band under illumination conditions (≥ 1 sun), the capacitive effect arises from the accumulation of excess minority carriers and is given by Eq. (9):

$$C_n = q^2 L \frac{dn}{dE_{Fn}} \tag{9}$$

where,

$$n = N_c e^{-(E_c - E_{Fn})/k_B T_c} \tag{10}$$

Here n, E_{Fn}, L, N_c and E_c represent the carrier concentration, electron quasi-Fermi level, thickness of solar cell, conduction band density of states and the conduction band edge energy respectively. The diffusion capacitance (C_n) depends on various parameters described by Eq. (9) to Eq. (10) and is expressed by Eq. (11) [21]:

$$C_n = \frac{\alpha q^2 L n_0}{k_B T_c} e^{\alpha q V_F}/k_B T_c \tag{11}$$

where, n_0 is the minority carrier density in equilibrium, α represents the contributions from trap levels (lies within the range from 0 to 1) [21,31].

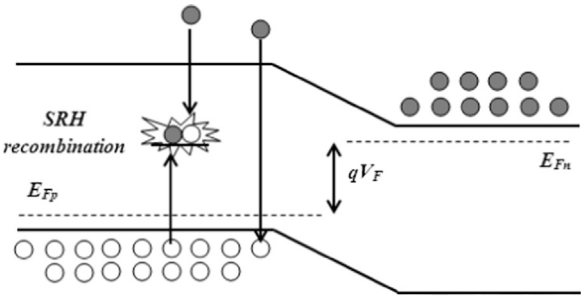

Fig. 3. The separation of the Fermi levels promoted the occupancies of the density of the states (DOS).

3. Experimental section

3.1. Device characterization

The solar cell I-V characterization was done using a solar simulator (Photoemission Tec SS80AAA with 1.5AM-G filter) and Source measuring unit (U2722A, Agilent). The temperature of the solar cell was measured by digital thermometer (MiniTemp, Raytek) with an accuracy of ± 2 °C and a Fresnel lens has been used for concentrating the solar radiation. During the measurement, the silicon solar cell was mounted on a heat sink to maintain a constant temperature. A three electrode potentiostat (CH Instruments 660D) equipped with a frequency response analyzer was used for impedance spectroscopy (IS) measurements. The working electrode was connected to the positive terminal of silicon solar cell (i.e. on back side) whereas the counter and reference electrode were shorted and connected to the negative front terminal of silicon solar cell. A variable dc voltage source is used to apply a potential difference from -0.5 to 1.0 V across the P-N junction with a scan rate of 5 mVs^{-1}. The inductive effect of connecting leads from Si solar cell to potentiostat has been taken care of during the experiments. IS data were collected in the form of Nyquist impedance spectra, and the high frequency components of series resistance were fully resolved. During IS measurement an A.C. perturbation signal of 5 mV root-mean-square voltage is applied in the frequency range of 1 Hz to 0.1 MHz.

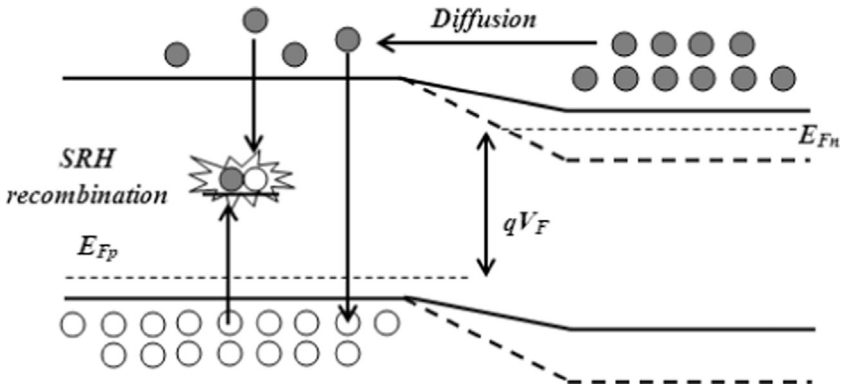

Fig. 4. The separation of the Fermi levels promoted the occupancies of the density of the states (DOS) under higher illumination.

3.2. Material aspects of polycrystalline Si solar cell

Commercially available polycrystalline Si solar cells procured from Nease Asia Pvt. Ltd. (India) were used in the present study. The solar cells are fabricated on p-type polycrystalline silicon wafers by $POCl_3$ diffusion and the electrical contacts on both the sides were made by screen-printing technology. These Si solar cells incorporate several material engineering aspects such as a back surface field (BSF) to reduce the recombination and a silicon nitride layer is used as an antireflective coating to minimize the reflection as well as surface passivation of the front surface. Fig. S1 (Supplementary Information) (a) shows the cross-sectional view of a polycrystalline Si solar cell with a thickness of $\approx$200 μm, isotropically etched topography of front surface (Fig. S1(b)) showing an average grain size of 2–3 μm with large grain size over 10 μm. Fig. S1(c) shows back surface layer of aluminum (25 μm). Fig. S1(d) shows the enlarged view of a current carrying finger having the width and height of 69 μm and 15 μm respectively. The photovoltaic characteristic parameters that is, short-circuit current (I_{SC}), open-circuit voltage (V_{OC}), fill factor (FF), and power conversion efficiency (η) of the solar cell (area: 0.512 cm^2) under 1 sun illumination (AM1.5, 1000 W/m^2) are 23 mA, 530 mV, 58.8% and 14%, respectively. The solar cell material parameters described here are used to explore the recombination kinetics by using impedance spectroscopy technique.

4. Results and discussion

4.1. Transport kinetics

From IS measurements, the influence of light concentration ($>$ 1 sun) on charge carrier recombination process and quasi-Fermi levels have been explored by applying a forward bias $V_F \approx V_{OC}$. The measurements were carried out on the polycrystalline silicon solar cell under different forward bias conditions and the impedance spectra are plotted (Fig. 5) in the complex plane (i.e. Z' versus Z", also known as Nyquist or Cole–Cole plot [32,33]). The transmission line model discussed in Section 2 is used to fit the Nyquist spectra (Fig. 5), where symbols and line represent the experimental data and theoretical fit, respectively. The Nyquist spectra obtained as a function of the applied bias lead to the following observations that is, (1) At low forward bias (FB) the resistance and capacitance of n^+-p junction are dominated by the shunt resistance (R_{SH}) and depletion layer capacitance (C_T), respectively, (2) As the FB across n^+-p junction increases, the radii of Nyquist spectra decreases, indicating the reduction in junction resistance. It must be noted here that the first two

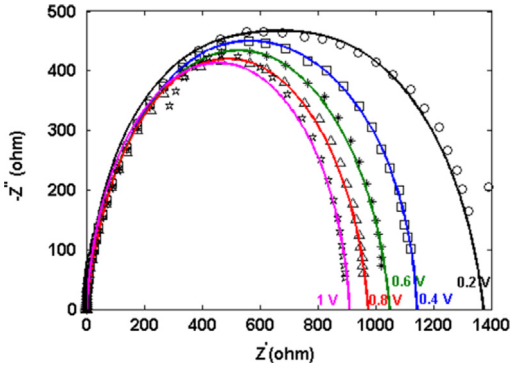

Fig. 5. The impedance spectrum of the polycrystalline Si solar cell for various bias voltages.

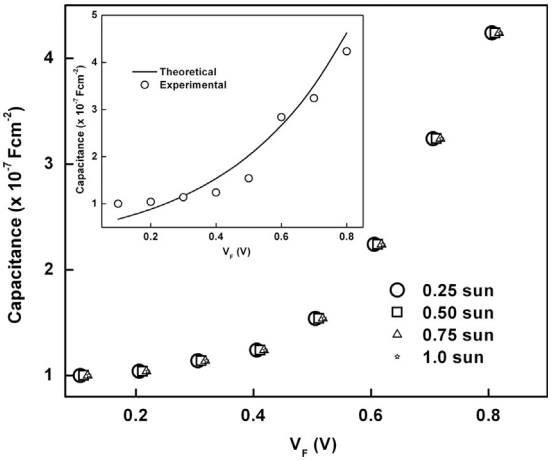

Fig. 6. Variation of C_μ as a function of voltage for various light intensities. The insert shows the variation of C_μ as a function of voltage in dark.

observations follow from the description of single time constant (Nyquist spectra below knee voltage of solar cell), and (3), as the junction bias increases beyond the knee voltage, the response of n^+-p diode junction shifts from high impedance to low impedance due to the switching of the charge accumulation mechanism in the SCR to the diffusion mechanism in the QNR. Fig. 6shows the variation of capacitive parameter C_μ extracted from the low frequency arc of the impedance spectra as a function of applied bias and light intensity. The obtained trend of C_μ as a function of intensity (Fig. 6) is similar to previous reports for silicon solar cell by other researchers [21,22]. The value of C_μ varies from 1×10^{-7} to 5×10^{-7} F/cm^2. The theoretical curve for the diffusion capacitance ($C_\mu \approx C_n$) is fitted for the data taken under dark conditions using Eq. (11) with the following constants: $n_0=1.10\times10^{10}$ cm^{-3}, L=200 μm, α=0.15 and T=300 K (insert of Fig. 6). At moderate and high forward bias condition, the diffusion capacitance ($C_\mu = C_0\exp(\alpha q V_F/k_BT)$) increases exponentially because of the occupation of electronic DOS by the excess minority charge carriers. The observed variation of diffusion capacitance with the applied bias indicates the electronic state distribution in the band gap and the displacement of the Fermi level. Under higher bias or at higher illumination condition, the introduction of excess extra holes (Δp) causes an insignificant change in the majority carriers (p_0). However, a small change in majority charge carrier causes the hole Fermi level to shift downward by $\Delta E_{F_p} = k_BT \ln p_0/(\Delta p + p_0)$, which is insignificant with respect to the shift of electron Fermi level. Since the electron carrier density in equilibrium is negligible, the electron Fermi level E_{F_n} changes significantly when excess carriers are generated at higher illumination level and this results in an exponential increase in the diffusion capacitance (C_μ).

Another important factor that influences the solar cell performance is the recombination process. The photo-generated electron-hole pairs can recombine before arriving to the contacts eventually reducing the maximum achievable efficiency of solar cell. The variation of diffusion resistance R_d extracted from the low frequency arc of the impedance spectra as a function of applied bias and illumination is shown in Fig. 7. The value of R_d varies from 0.5 to 770 Ω-cm^2 under dark conditions. From Fig. 7, it can be observed that the diffusion resistance follows an exponential behaviour given by $R_d = R_0\exp(-qV_F/n_1k_BT)$. The general parameters used for the theoretical fitting (insert of Fig. 7) of diffusion resistance (R_d) are: R_0=1350 Ω-cm^2, n_1=2.2 and T=300 K.

An effective carrier lifetime ($\tau_n = R_d(V)sC_\mu(V)$) determined from the low frequency arc of the impedance spectra as a function of charge carrier density is shown in Fig. 8. The steady state carrier

density can be calculated by integrating the diffusion capacitance and is given by:

$$n = \frac{1}{qL}\int_0^{V_{OC}} C_\mu(V)\, dV \tag{12}$$

The effective carrier lifetime lies within the range of 20–100 μs (for $V_{OC} > 0.4\ V$) and decreases as the carrier density increases with illumination (Fig. 8). Three distinct regions are observed on the charge carrier density versus effective carrier lifetime curve. The first region in Fig. 8shows the effective lifetime moderately decreasing as carrier density increases, for smaller carrier densities. The carrier density is approximately proportional to the light intensity under low illumination, so the lifetime remains constant with photo-generation rate. The second region elucidates that the polycrystalline silicon solar cell can be operated under concentrated illumination conditions (from >1 sun to $\approx$ 3.3 suns) with a compromise in the effective lifetime of electrons. The effective lifetime decreases due to the onset of flat-band potential which enhances the diffusion driven transport of charge carriers leading to an increased recombination rate. The third region indicates a high recombination region, wherein the commercially available polycrystalline silicon solar cell cannot be operated efficiently ($>$ 3.3 suns). For a monocrystalline Si solar cell, a similar effective lifetime versus charge density plot at higher charge injection level has been reported by other authors [34]. The underlying mechanism of this effect has been explained in terms of dominance of Auger recombination over SRH and radiative recombination. These observations indicate that polycrystalline silicon solar cells can be used for low concentration photovoltaic applications ($\approx$ 3 suns). The above mentioned parameters that is, diffusion capacitance, diffusion resistance, effective charge carrier lifetime represent semiconductor's material aspects which are important in the analysis of the performance of a silicon solar cell under illuminated conditions.

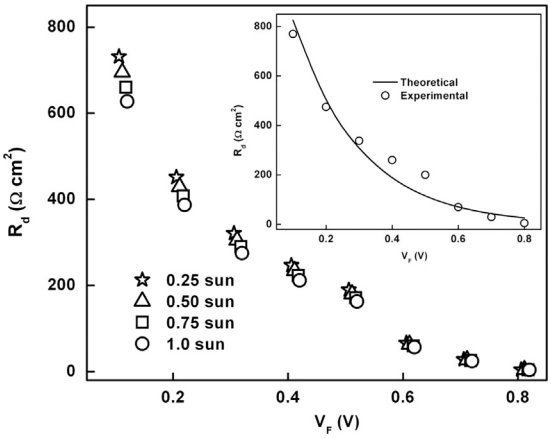

Fig. 7. Diffusion resistance (R_d) as a function of applied bias for various light intensities. The insert shows the variation of R_d as a function of voltage in dark.

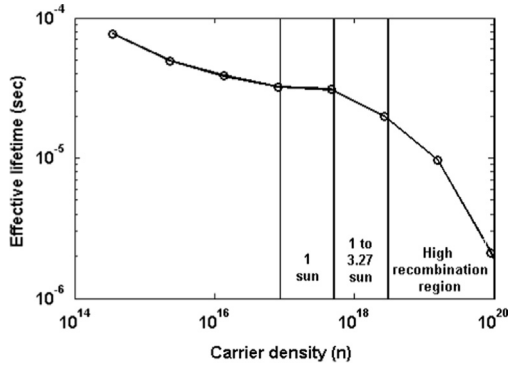

Fig. 8. Carrier density versus effective lifetime for ploy-crystalline silicon solar cell.

4.2. Effect of illumination on current-voltage characteristics

The static parameters (I_{SC}, V_{OC}, FF and efficiency η) of the polycrystalline silicon solar cell are measured under STC and low concentration conditions. These parameters are calculated using the model discussed in Section 2 and the various parameters used to simulate the experimental data are listed in Table 1. The extracted device parameters from theoretical fitting of experimental data are listed in Table 2. A plot having measured and simulated current-voltage curves for all the CR values is shown in Fig. 9. The measured values of solar irradiation, I_{SC} and V_{OC}, as a function of CR are plotted in Fig. 10. From the insert of Fig. 10, a linear relationship between the output current of polycrystalline silicon solar cell and CR is observed. This increasing trend of output current with an increase in illumination is consistent with the observation of other authors [12,35].

In an ideal case, where the transport mechanism does not severely limit the solar cell performance, Eq. (8) can be used as a starting point to derive the achievable V_{OC}. The difference between

Table 2
The parameters extracted from fitted curve.

CR	R_S (Ω)	n_1	n_2	I_i (A)	I_r (A)
1	1.4	2.4	4.8	3.38×10^{-6}	2.85×10^{-4}
2.77	1.4	2.4	4.8	3.38×10^{-6}	2.85×10^{-4}
3.27	1.7	2.1	4.9	9.56×10^{-7}	3.12×10^{-4}
4	1.9	1.5	5.0	1.67×10^{-8}	3.41×10^{-4}
5	2.0	1.3	5.2	1.89×10^{-9}	4.03×10^{-4}

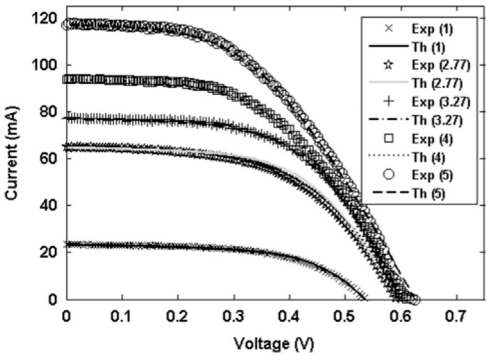

Fig. 9. Current-voltage characteristics of polycrystalline silicon solar cell with varying illumination levels (1 sun corresponds to AM1.5, 1000 W/m^2) (The R_S values used for theoretical fitting are given as 1.4 Ω, 1.4 Ω 1.7 Ω 1.9 Ω and 2.0 Ω for 1 sun, 2.77 sun, 3.27 sun, 4 sun and 5 sun, respectively). 'Exp' and 'Th' represent experimental and theoretical respectively.

Table 1
The fitting parameters used for simulation.

Module Parameter	E_g (eV)	A (cm^2)	T_c (K)	T_{ref}(K)	k_B (J/K)	K_I	q (C)	I_{SC} (A)	R_{SH} (Ω)	V_{OC} (V)
For 1 sun	1.12	0.512	298	298	1.38×10^{-23}	0.65×10^{-3}	1.602×10^{-19}	0.0235	800	0.53

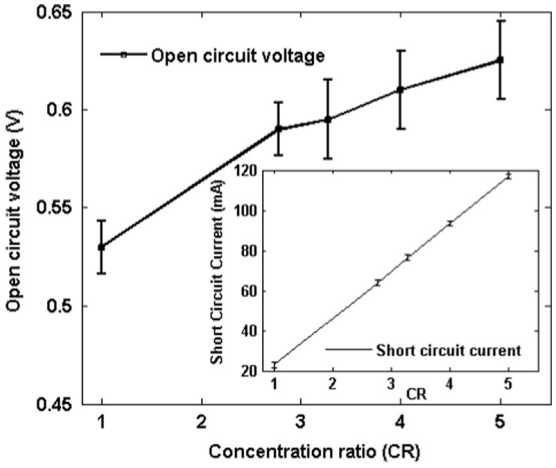

Fig. 10. Open circuit-voltage characteristics of polycrystalline silicon solar cell with varying illumination levels. The insert shows variation of short circuit current with illumination levels. A ± 3% deviation is observed in experimental data compared to theoretical calculations (shown by error bar).

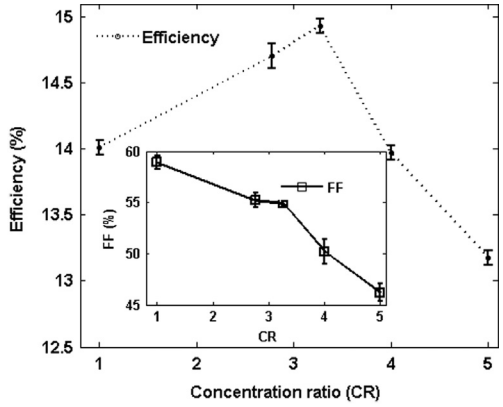

Fig. 11. Efficiency of polycrystalline silicon solar cell with varying illumination levels. The insert shows the variation of fill factor (FF) with illumination levels.

electron and hole Fermi level gives the open-circuit voltage (V_{OC}), which increases with increasing illumination level (> 1 sun, AM1.5 solar spectrum) at constant temperature. A similar increasing trend of V_{OC} with CR is observed practically as shown in Fig. 10 with ± 3% acceptable deviation in experimental and theoretical data. The trend of V_{OC} with CR is comparable to those shown in Fig. 4 of reference [36] and Fig. 2 of reference [37]. In Fig. 9, maximum power point (MPP) shifts towards the lower voltage with the increase in CR. This shift in MPP at higher illumination level is mainly attributed to the enhanced recombination of carriers governed by diffusion transport in the conduction band under flat-band condition. The plot shown in Fig. 11 describes the dependence of η and FF (insert of Fig. 10) of polycrystalline Si solar cell with the change in CR. From Fig. 11 it is observed that the efficiency of polycrystalline Si solar cell increases to a maximum of 14.8% at CR ≈ 3.27 suns and then decreases with the increase in CR. The increase in efficiency with CR is mainly attributed to the following reasons: (1) the excess electron-hole pair generated under concentration are efficiently collected across the fingers and bus bars due to an insignificant decrease in effective carrier lifetime until 3.27 suns (Figs. 8); and (2) the occupation of minority charge carriers in conduction band results in the shift of quasi-Fermi levels at p-side and n-side of the junction, leading to an increase in V_{OC} at constant temperature. At higher CR or beyond 3.27 suns, the aforementioned effects are minimized and a combination of I^2R_S loss and changes in the diode quality factors causes a reduction in efficiency of Si solar cell [38,39]. With the increase in CR, higher R_S in the active layer results in power losses equivalent to I^2R_S in the polycrystalline solar cell and thus reduces its performance. The value of R_S increases from 1.4 Ω to 2 Ω with the change in CR from 1 to 5 suns respectively. A similar trend of R_S with illumination for Si solar cell is observed by other researchers [40,41] and the physical origin is explained as the charging of grain boundaries, which hinder the charge carriers [42]. The increase in the value of R_S with the change in CR leads to a higher voltage drop within the solar cell. This effect eventually reduces the FF as observed in Fig. 11 (inset). A similar variation of FF with the increase in CR for polycrystalline Si [35] and chalcopyrite solar cell [43] is observed by other researchers. In contrast to the polycrystalline Si, monocrystalline Si solar cell shows an increase in FF with illumination up to optimum CR and then a decrease with further increase in CR [39]. A difference in the behaviour of these technologies with CR is attributed to the functional dependence of FF on R_{SH} and R_S. Under low CR, a lower value of $R_{SH} \sim 800\ \Omega$ for polycrystalline Si, as compared to the $R_{SH} \sim 10^4\ \Omega$ for monocrystalline Si solar cell [39], causes greater power loss in polycrystalline Si solar cell by providing an alternate current path for the light generated current. Such a diversion reduces the amount of current flowing through the solar cell resulting in the reduction of FF and junction voltage [38]. With the change in R_{SH}, the reduction in FF is given by: $FF = FF_0(1-1/R_{SH})$ [38], where FF_0 represents the FF without any parasitic losses. The values of R_S for monocrystalline and polycrystalline Si solar cells vary from 0.02–0.80 Ω from 1 sun to ~12 suns [39] and 1.4–2.0 Ω from 1 sun to 5 suns respectively. With increase in CR, the higher value of R_S for polycrystalline Si solar cell causes a larger voltage drop as compared to monocrystalline Si resulting in the decrease of FF as given by: $FF = FF_0(1-R_S)$ [38].

From the model discussed in Section 2 (Eqs. (5) and (6)), it can be observed that the increase in the value of CR (denominator of Eq. (6)) is compensated by the linear increase in the value of I_{SC} (numerator of Eq. (5)) and the efficiency seems to increase with the increase in V_{OC} up to optimum concentration. Thus, beyond the optimum CR, the reduction in the value of FF is comparatively higher than the increase in V_{OC} which leads to the reduction in η of Si solar cell. The dominance of recombination current is another factor for the lower value of η. According to the Shockley-Read-Hall recombination effect, an ideality factor (n_2) should be approximately equal to 2 if recombination in SCR takes place for an ideal device. A higher value of $n_2 > 2$ is often observed for industrial solar cells [44]. On the other hand, an ideality factor (n_1) equal to 1 at high FB signifies a diffusion of charge carriers in the QNR. In this study the value of diode ideality factor, n_1 is fitted as 2.4 for 1 sun illumination, which indicates that the current transport is controlled by either exponentially distributed trap states in the absorber band gap or by recombination in bulk QNR [35]. Further, the value of n_2 is fitted as 4.8 for 1 sun illumination, which is associated with the high density of electrically active defect states at the grain boundaries leading to direct [45] or tunnelling assisted recombination [46]. The extracted parameters from I-V plot listed in Table 2 show a decrease in the value of n_1 and I_i with the increase in CR, which is consistent with the previous reports on polycrystalline Si solar cell and heterojunction devices [35,43]. The decrease in n_1 and I_i is attributed to the deactivation of recombination defects in the band gap [35,45] due to the shift of electron quasi-Fermi level towards the conduction band edge as shown in Fig. 4. On the other hand, an increase in n_2 and I_r with increase in CR indicates the increase in the number of electrically active defect states at the grain boundaries leading to the recombination of photogenerated charge carriers similar to interface recombination discussed by other researchers [35,45]. From the aforementioned discussions, it can be concluded that an increase in η with the change in CR depends on the increase in V_{OC} of a solar cell whereas a linear increase in the value of R_S along

with the dominance of recombination causes a reduction in η- beyond the optimum CR. A similar study for commercially available mono-crystalline silicon solar cells under varying illumination conditions has been reported recently [39].

5. Conclusions

Commercially available polycrystalline silicon solar cells have been studied under varying illumination conditions to explore their application to a low-concentration photovoltaic system. On the basis of this study, it can be concluded that charge carrier recombination is closely related to the increase in carrier density with the increase in illumination. The electrical performance of a polycrystalline silicon solar cell is limited by the recombination losses which limit the attainable open-circuit voltages. The losses get proportionately larger at higher illumination. It is emphasized that under higher illumination levels the charge transport is mainly governed by a diffusion process, which leads to increased recombination of charge carriers and a decrease in the fill factor of polycrystalline silicon solar cells. The work reported a detailed analytical framework for the determination of a broad range of performance indicating parameters (diffusion capacitance, diffusion resistance and effective lifetime) of polycrystalline silicon solar cell based on an impedance spectroscopy technique. The impedance measurements show that the diffusion capacitance varies from 1×10^{-7} F/cm^2 to 5×10^{-7} F/cm^2 and diffusion resistance varies from 0.5 to 770 Ω-cm^2 with bias. This study indicated that the commercially available polycrystalline Si solar cell works efficiently under low concentration $\approx$ 3 suns.

Acknowledgement

The authors are deeply grateful to Dr. G. P. Smestad and anonymous referees for their invaluable suggestions to improve the quality of this article. Authors acknowledge Prof. Indrajit Mukhopadhyay for his continuous guidance and technical discussions.

Appendix A. Supporting information

Supplementary data associated with this article can be found in the online version at http://dx.doi.org/10.1016/j.solmat.2014.10.031.

References

[1] V.A. Chaudhari, C.S. Solanki, From 1 Sun to 10 suns c-Si cells by optimizing metal grid, metal resistance, and junction depth, Int. J. Photoenerg. (2009) http://dx.doi.org/10.1155/2009/827402.
[2] C.S. Solanki, Solar Photovoltaics: Fundamental, Technologies and Applications, second ed., Prentice Hall, India, 2011.
[3] I.A. Schwirtlich, EFG ribbon technology, in: V. Petrova-Koch, R. Hezel, A. Goetzberger (Eds.), High-Efficient Low-Cost Photovoltaics, Springer Series in Optical Sciences, 140, Springer, Berlin, Germany, 2009, pp. 57–64.
[4] B. Pivac, V. Borjanovi, I. Kovacevi, B.N. Evtody, E.A. Katz, Comparative studies of EFG poly-Si grown by different procedures, Sol. Energ. Mater. Sol. Cell. 72 (2002) 165–171.
[5] P.A. Basore, CSG-1: manufacturing a new polycrystalline silicon PV technology, Proceedings of the 4th IEEE World Conference on Photovoltaic Energy Conversion (WCPEC'07) 2, 2007, pp. 2089–2093.
[6] A. Cuevas, R.A. Sinton, N.E. Midkiff, R.M. Swanson, 26-percent efficient point-junction concentrator solar cells with a front metal grid, Electron Devic. Lett. 11 (1990) 6–8.
[7] Y. Tripanagnostopoulos, M. Souliotis, S. Tselepis, V. Dimitriou, ThMakris, Design and performance aspects for low concentration photovoltaics, 20th EUPVSEC, 6–10 June, Barcelona, Spain (2005).
[8] A. Luque, V. Andreev, Concentrator Photovoltaics (Chapter: 1 and 6), first ed., Springer, Berlin, Heidelberg, New York, 2007.
[9] B. Tripathi, P. Yadav, M. Lokhande, M. Kumar, Feasibility study of commercial silicon solar PV module based low concentration photovoltaic system, Int. J. Elec. Electron. Eng. Res. 2 (2012) 84–93.
[10] S. Kurtz, Opportunities and challenges for development of a mature concentrating photovoltaic power industry, Technical Report, NREL/TP-520- 43208, 2009.
[11] P. Yadav, B. Tripathi, M. Kumar, Exergy, energy and dynamic parameter analysis of indigenously developed low concentration photovoltaic system, Int. J. Photoenergy (2013)http://dx.doi.org/10.1155/2013/929235.
[12] A. Zahedi, Review of modelling details in relation to low-concentration solar concentrating photovoltaic, Renew. Sust. Energ. Rev. 15 (2011) 1609–1614.
[13] G. Sala, I. Anton, J. Monedero, P. Valera, M.P. Friend, M. Cendagorta, F. Perez, E. Mera, E. Camblor, The euclides-thermie concentrator power plant in continuous operation, Proceedings of the 17th EUPVSEC, Munich, Germany (2001) 488–491.
[14] F. Reis, M.C. Brito, V. Corregidor, J. Wemans, G. Sorasio, Modeling the performance of low concentration photovoltaic systems, Sol. Energy Mater. Sol. Cell. 94 (2010) 1222–1226.
[15] P. Yadav, B. Tripathi, M. Lokhande, M. Kumar, Effect of temperature and concentration on commercial silicon module based low-concentration photovoltaic (LCPV) system, AIP J. Renew. Sust. Energ. 5 (2013) (013113-1-10).
[16] P. Yadav, B. Tripathi, M. Lokhande, M. Kumar, Estimation of steady state and dynamic parameters of low concentration photovoltaic system, Sol. Energy Mater. Sol. Cell. 112 (2013) 65–72.
[17] M. Castro, I. Anton, G. Sala, Pilot production of concentrator silicon solar cells: approaching industrialization, Sol. Energ. Mater. Sol. Cell. 92 (2008) 1697–1705.
[18] M. Li, X. Ji, G. Li, S. Wei, Y. Li, F. Shi, Performance study of solar cell array based on a trough concentrating photovoltaic/thermal system, Appl. Energ. 88 (2011) 3218–3227.
[19] M.A. Schuetz, K.A. Shell, S.A. Brown, G.S. Reinbolt, R.H. French, R.J. Davis, Design and construction of a ~7× low-concentration photovoltaic system based on compound parabolic concentrators, IEEE J. Photovoltaics (2012), http://dx.doi.org/10.1109/JPHOTOV.2012.2186-283.
[20] P. Yadav, B. Tripathi, S. Rathod, M. Kumar, Real-time analysis of low-concentration photovoltaic systems: a review towards development of sustainable energy technology, Renew. Sust. Energ. Rev. 28 (2013) 812–823.
[21] I. Mora-Sero, G. Garcia-Belmonte, P.P. Boix, M.A. Vazquez, J. Bisquert, Impedance spectroscopy characterization of highly efficient silicon solar cells under different light illumination intensities, Energ Environ. Sci 2 (2009) 678–686.
[22] J.E. Garland, D.J. Crain, J.P. Zheng, C.M. Sulyma, D. Roy, Electro-analytical characterization of photovoltaic cells by combining voltammetry and impedance spectroscopy: voltage dependent parameters of a silicon solar cell under controlled illumination and temperature, Energ. Environ. Sci 4 (2011) 485–498.
[23] D. Ding, S.R. Johnson, S.Q. Yu, S.N. Wu, Y.H. Zhang, A semi-analytical model for semiconductor solar cells, J. Appl. Phys. 110 (2011) 123104.
[24] M. Veerachary, T. Senjyu, K. Uezato, Voltage-based maximum power point tracking control of PV system, IEEE T. Aerosp. Electron. Syst. 38 (2002) 262–270.
[25] M. Veerachary, K.S. Shinoy, V2-based power tracking for nonlinear PV sources, IEE P.-Elec. Power Appl. 152 (2005) 1263–1270.
[26] I.S. Kim, M.J. Youn, Variable-structure observer for solar array current estimation in a photovoltaic power-generation system, IEE P.-Elec. Power Appl. 152 (2005) 953–959.
[27] I.S. Kim, M.B. Kim, M.J. Youn, New maximum power point tracker using sliding-mode observer for estimation of solar array current in the grid-connected photovoltaic system, IEEE T. Ind. Electron. 53 (2006) 1027–1035.
[28] S.S. Li, Semiconductor Physical Electronics, Plenum Press, New York, 1993.
[29] J. Nelson, The Physics of Solar Cells, Imperial College Press, London, 2004.
[30] H.L. Tsai, C.S. Tu, Y.J. Su, Development of generalized photovoltaic model using MATLAB/SIMULINK, Proceedings of the World Congress on Engineering and Computer Science, San Francisco, USA, 2008.
[31] G. Garcia-Belmonte, A. Guerrero, J. Bisquert, Elucidating operating modes of bulk-heterojunction solar cells from impedance spectroscopy analysis, J. Phys. Chem. Lett. 4 (2013) 877–886.
[32] S. Kumar, P.K. Singh, G.S. Chilana, S.R. Dhariwal, Generation and recombination lifetime measurement in silicon wafers using impedance spectroscopy, Semicond. Sci. Technol. 24 (2009) 095001–095008.
[33] K. Pandey, P. Yadav, I. Mukhopadhyay, Elucidating different mass flow direction induced polyaniline–ionic liquid interface properties: insight gained from DC voltammetry and impedance spectroscopy, J. Phys. Chem. B. 118 (2014) 3235–3242.
[34] C. Battaglia, S.M. Nicolas, S.D. Wolf, X. Yin, M. Zhang, C. Ballif, A. Javey, Silicon heterojunction solar cell with passivated hole selective MoO_x contact, Appl. Phys. Lett. 104 (2014) 113902–113905.
[35] A. Kassis, M. Saad, Analysis of multi-crystalline silicon solar cell at low illumination levels using a modified two-diode model, Sol. Energ. Mater. Sol. Cell. 94 (2010) 2108–2112.
[36] F. Khan, S.N. Singh, M. Husain, Effect of illumination intensity on cell parameters of a silicon solar cell, Sol. Energ. Mater. Sol. Cell. 94 (2010) 1473–1476.
[37] B. Gupta, P.K. Shishodia, A. Kapoor, R.M. Mehra, T. Soga, T. Jimbo, M. Umeno, Effect of illumination intensity and temperature on the I-V characteristics of n-C/p-Si heterojunction, Sol. Energ. Mater. Sol. Cell. 73 (2002) 261–267.
[38] ⟨http://www.pveducation.org/pvcdrom/solar-cell-operation/⟩ (accessed 02.07.14).
[39] P. Yadav, B. Tripathi, K. Pandey, M. Kumar, Recombination kinetics in a silicon solar cell at low concentration: electro-analytical characterization of space-charge and quasi-neutral regions, Phys. Chem. Chem. Phys. 16 (2014) 15469–15476.

[40] A. Kassis, M. Saad, Analysis of multi-crystalline silicon solar cells at low illumination levels using a modified two-diode model, Sol. Energ. Mater. Sol. Cell. 94 (2010) 2108–2112.
[41] J.C. Wang, J.C. Shieh, Y.L. Su, K.C. Kuo, Y.W. Chang, Y.T. Liang, J.J. Chou, K.C. Liao, J.A. Jiang, A novel method for the determination of dynamic resistance for photovoltaic modules, Energy 36 (2011) 5968–5974.
[42] S.E. Lee, D.G. Lim, Y. Yi, Novel type of multicrystalline silicon solar cell with an additional electrode along the grain boundaries, J. Korean Phys. Soc. 37 (2000) 64–68.
[43] H. Bayhan, M. Bayhan, A simple approach to determine the solar cell diode ideality factor under illumination, Sol. Energ. 85 (2011) 769–775.
[44] O. Breitenstein, J. Bauer, A. Lotnyk, J.M. Wagner, Defect induced non-ideal dark I-V characteristics of solar cells, Superlattice Microstruct. 45 (2009) 182–189.
[45] M. Saad, A. Kassis, Effect of interface recombination on solar cell parameters, Sol. Energ. Mater. Sol. Cell 79 (2003) 507–517.
[46] A. Kassis, M. Saad, Separation of solar cell current into its constituent parallel currents under illumination, Renew. Energ. 33 (2008) 974–978.